Published in final edited form as:
Exp Eye Res. 2010 October ; 91(4): 513–523. doi:10.1016/j.exer.2010.07.007.

Mapping the entire human corneal nerve architecture

Jiucheng He, **Nicolas G. Bazan**, and **Haydee E.P. Bazan**
Neuroscience Center of Excellence and the Department of Ophthalmology Louisiana State University Health Sciences Center, School of Medicine, New Orleans, Louisiana, USA

Abstract

We developed an approach to generate a three-dimensional map that facilitates the assessment of epithelial nerve density in different corneal areas to define aging and gender influence on human corneal nerve architecture. Twenty-eight fresh human eyes from 14 donors of different ages were studied. Corneal nerves were stained and consecutive images acquired with a fluorescence microscope, recorded at the same plane, and merged for viewing the complete epithelial and stromal nerve architecture. After whole mount examination, the same cornea was also used for transection. Stromal nerves entered the cornea in a radial pattern, subsequently dividing into smaller branches. Some branches connected at the center of the stroma, but most penetrated upward into the epithelium. No differences were observed between nerve densities in the four corneal quadrants. Epithelial innervation in the limbal and most of the peripheral area was supplied by a superficial network surrounding the limbal area. Central epithelial nerves were supplied by branches of the stromal nerve network. Epithelial nerve density and terminal numbers were higher in the center of the cornea, rather than the periphery. There were no differences in epithelial nerve density between genders, but there was a progressive nerve density reduction concomitant with aging, mainly in eye samples of donors 70-years of age and older. The modified technique of tissue preparation used for this study allowed for observation of new nerve structure features and, for the first time, provided a complete view of the human corneal nerve architecture. Our study reveals that aging decreases the number of central epithelial nerve terminals, and increases the presence of irregular anomalies beneath the basal layer.

Keywords

stromal nerves; epithelial nerves; aging of corneal nerves; gender and corneal nerves; immunofluorescence of corneal nerves

1. Introduction

The organization of human corneal nerves has been studied since their discovery in the limbus by Schlemm in 1831 (Schlemm, 1831). A renewed interest in corneal neurobiology arose recently because of the pivotal role these nerves play in maintaining a healthy ocular surface, which is especially important today due to the damage corneal nerves incur from refractive surgery, corneal transplants and herpetic infections. One major condition that causes epithelial

Corresponding author: Haydee E.P. Bazan, Department of Ophthalmology and Neuroscience Center of Excellence, Louisiana State University Health Sciences Center, 2020 Gravier St., Suite D., New Orleans, LA70112, USA; Tel: (504) 599-0877; Fax: (504) 568-5801; hbazanl@lsuhsc.edu.

Disclosure: J. He, None; N.G. Bazan, None; H.E.P. Bazan, None

abnormalities is dry eye syndrome. It is calculated that nearly 10% of the U.S. population suffers from dry eye syndrome, which significantly affects quality of life. Incidence of dry eye increases with aging (Smith, 2007) and although some risk factors have been identified, the causes are still largely unknown. It is important, therefore, to determine how aging affects the nerve architecture of the cornea.

Earlier studies on corneal nerves in animal and human corneas have been based primarily on light or electron microscopy. The first detailed description of epithelial nerves was made after studying fresh central corneal buttons from enucleations and keratoplasties stained with gold chloride (Schimmelpfennig, 1982). Since then, different staining and fixation techniques and a variety of analytic methods have increased information on the morphology, ultrastructural organization, density, and postmortem changes of corneal nerves (Auran et al., 1995; Müller et al., 1996; Müller et al., 1997; Ueda et al., 1989). More recently, *in vivo* confocal microscopy (IVCM) has provided an opportunity for non-invasive examination of living human corneas at the cellular level (Lee et al., 2002; Malik et al., 2003; Oliveira-Soto and Efron, 2001; Patel and McGhee, 2005; Patel and McGhee, 2009; Stachs et al., 2007; Scarpa et al., 2008). However, the distribution of corneal nerves is not completely understood (Müller et al., 2003) because: 1) conventional histology requires fresh corneas and are unable to show detailed innervations of the corneal layers; 2) images obtained by transmission electron microscopy have been limited to very small areas of the corneal surface (0.1 mm^2 maximum); 3) IVCM images of the human cornea are recorded preferentially from the corneal apex; and most importantly, 4) nerve branches and terminals of less than 0.5 μm in diameter cannot be imaged with the *in vivo* confocal microscopes, tandem scanning confocal microscopes, or scanning slit confocal microscopes currently available.

Here we describe a modified method of immunofluorescence staining and imaging that reveals details of the epithelial and stromal nerve networks in two dimensions and provides transected views of the whole corneal nerve network. This approach, for the first time, allows for detailed mapping of the entire human corneal nerve architecture and identification of changes in central corneal epithelial nerve densities during aging. Preliminary studies were presented in ARVO (He et al., 2009).

2. Materials and methods

2.1 Human Eye Specimens

This study was conducted according to the tenets of the Declaration of Helsinki. Twenty-eight fresh human eyes from four females (aged 44, 54, 57, and 79 years old) and ten males (aged 19, 40, 45, 52, 57, 63, 66, 67, 75, and 80 years old) were obtained from the National Disease Research Interchange (NDRI). The eyes were kept in a wet chamber and shipped to our laboratory on ice. The donors had no history of eye disease, contact lens wear, ocular surgery, or systemic diseases that might have affected the cornea. Before use in this study, eyes were examined by slit lamp biomicroscopy and surgical microscopy, and all corneas were confirmed to be clinically normal. The average time interval between death and fixation was 36 ± 11 hours (Mean ± SD).

2.2. Tissue preparation, Immunofluorescence Staining and Imaging

Corneas were excised along the sclero-corneal rim. The endothelium, which was used for other purposes, was removed together with the Decemet's membrane using a tooth-free fine forceps under a dissection microscope. To obtain a whole mount view of the entire epithelial nerve architecture, the position of the cornea was defined before dissecting the tissue according to the position of the optic nerve and the attachment sites of the extraocular muscles. Marks were made on the endothelial side of the limbus using a blade tip. The corneas were fixed in freshly-

prepared 4% paraformaldehyde for 24 hours at 4°C. Following three washes with 0.1M PBS containing 0.1% bovine serum albumin (PBS-BSA), corneas were placed in a 24-well plate (one cornea/well) and then incubated with 10% normal goat serum plus 0.3% Triton X-100 solution in PBS-BSA for 60 minutes at room temperature to block nonspecific binding. Afterwards, each cornea was incubated with a mouse monoclonal anti-βIII-tubulin antibody (Tuj1, MMS-435P, a monoclonal antibody specific for neuronal class βIII tubulin, 1:3000, Convance Antibody Services Inc, Berkeley, CA) in 0.1M PBS containing 1.5% normal goat serum + 0.1% Triton X-100 for 72 hours at 4°C and shaken constantly. After washing with PBS-BSA (4 × 15 minutes), corneas were incubated with the secondary antibody Alexa Fluor® 488 goat anti-mouse IgG (1:1500, Molecular Probes, Eugene, Oregon) for 24 hours at 4°C (shaken constantly), and then washed with PBS-BSA thoroughly. Previous studies omitting the first antibody showed no staining (Cortina et al., 2010; Esquenazi et al., 2005).

After staining, corneas were mounted in a bottle cap with a central hole of 12.5 mm interior diameter to maintain the natural shape of the tissue. The cap was inversely positioned in a well of a 24-well plate in which the bottom had been marked with one vertical and one horizontal line crossing the center of the well. The apex of the cornea was positioned at the cross point. The well was filled with 0.1M PBS to cover the cornea. Consecutive images, from the center to the periphery as well as from the anterior to the posterior cornea, were acquired using a time-lapse mode by focusing on different layers at various times; a fluorescence microscope (Nikon Eclipse TE200) equipped with a Photometrics digital camera (CoolSNAP™ HQ) using MetaVue imaging software was used. The images, which were recorded on the same plane at adjoining points, were merged using Photoshop imaging software (Adobe, Mountain View, CA) and then pasted onto a Microsoft Office PowerPoint template to build the whole view of the corneal epithelial nerve architecture.

To acquire the whole image of the stromal nerve structure, consecutive images were captured by a stereoscopic zoom microscope (Nikon SMZ 1500) set at a low magnification of 4× (objective lens). Images were merged to build a complete view of corneal stromal nerves as described above. The number of stromal nerves in each cornea was determined by counting the thick nerve trunks at the corneo-scleral limbus on the entire image of the stromal nerve distribution.

To get transected images of corneal nerves, the same corneas, after whole mount examination, were randomly cut into two halves and embedded in optimal cutting temperature (OCT) compound (Sakura Finetek USA, Inc, Torrance, CA). Serial 20-μm cryostat sections were cut, air-dried, and stored in the dark. For better visualization of epithelial nerves, the cuts were made a little obliquely, as previously described (Cortina MS et al., 2010). The sections were used directly or kept at −80°C for up to six months without obvious changes. When in use, the sections were washed in 0.1M PBS to remove OCT, counterstained with 4′-6-Diamidino-2-phenylindole (DAPI), and then covered with a mounting medium (Aqua-Mount; Lerner Laboratories, Pittsburgh, PA). Images were captured using the same microscope as above.

2.3. Data Analysis

Because human corneas have a radius of about 6 mm, epithelial innervation densities were determined based on an area 3 mm thick starting at the apex (the central zone) and an area 2 mm thick beginning at the limbus (the peripheral zone), with a 1 mm space left uncounted between them (the transition zone) to avoid overlap and confusion. Images were taken at a magnification of 20× from each of the four quadrants within these zones, as described above. To get a better contrast, the fluorescent images were changed to grayscale mode and placed against a white background using Photoshop imaging software. The nerve fibers of each image were carefully drawn with four-pixel lines following the course of each fiber. Nerve area percentage was quantified for each image using the image analysis program. To compare nerve

densities in the central and peripheral areas, 8 images of each zone were randomly chosen from each cornea (2 images/quadrant). A total of 80 images for each zone from 10 corneas were averaged. The nerve bundles were counted at the point where the nerves penetrated from the stroma to the epithelia. Nerve terminals in superficial epithelia within the central and peripheral zones were calculated by directly counting the number of terminals in each image (20× magnification). Differences in central and peripheral corneal nerve densities and terminal numbers were compared by analysis of variance (ANOVA); $p<0.05$ was considered a statistically significant difference.

3. Results

3.1. Stromal Nerve Architecture

Corneal stromal nerves originate from the sclera or ciliary body. A transverse section in Figures 1a and 1b show human stromal nerves (SN) entering from the sclera (S) to the peripheral (P) corneal stroma. Figure 1c shows dense innervation in the sclera around the limbus, with nerves running horizontally towards the stroma. Once in the stroma, the nerves divided into smaller branches, and most of the branches penetrated into the epithelium to form the epithelial nerve network at the peripheral cornea (Fig. 1d, e). A mounted complete view of the stromal nerve distribution of a normal cornea from a 45-year-old male donor (Fig. 1f) shows the nerves penetrating the stroma in a radial pattern. There are some nerves that connected at the central area, forming a stromal nerve network, and a small proportion of these nerves reached the epithelium.

The number of stromal nerve trunks range was calculated as an average of 32.6 ± 6.4 ($n = 10$, ages 40–57 years old). There was a 19% disparity in the number of stromal nerves between the examined corneas (range: 26–41). However, this difference did not correlate with the age or the gender of the donors. No significant differences were found between the number of nerves in each of the four quadrants of the cornea (Fig. 1g).

3.2. Corneal Epithelial Nerve Architecture

Epithelial innervation is supplied by two nerve networks. The first is the limbal superficial nerve network (LSNN) (Fig. 2a), which is an extension of the sub-conjunctiva nerve network (SCNN), and forms a dense network within the epithelium and anterior stroma (Fig. 2a, b). Fine nerve bundles emerging from this network innervate the limbal area and most of the peripheral area. In Figure 2c-f, the nerve structure in the limbal area can be seen at different depths from the superficial epithelial nerves running as fine nerve bundles to the deep stromal nerve trunks. A large number of dendritic cells (DC), which stained positive with anti-βIII-tubulin antibody, were seen in the epithelial layer surrounding the limbal area (Fig. 2b, c). These cells also were abundant in the conjunctival epithelium (CE), but few were found in the clear cornea. The second network originated from the branches of the peripheral stromal nerves. The tips of the stromal nerve branches penetrated the Bowman's layer into the epithelium (Fig. 2g, arrows), these nerve tips gave rise to long bundles (Fig. 2h) that ran from the periphery to the center close to the subbasal epithelia like wavy lines.

As shown in the whole view image of the epithelial nerves (Fig. 3a), nerves penetrated predominantly in the peripheral area. Along their course, these long nerve bundles divided into numerous smaller branches that connected to each other, constituting a delicate nerve network within the epithelium (Fig. 3b, c). Fine terminals or free endings budding from the network innervated the epithelial cells (Fig. 3d). Some of the terminals were longer than others and branched once or twice before ending. The average number of bundles per human cornea was 351 ± 53.5 (range: 312–430, $n = 7$, ages 40, 44, 45 and 54 years old). In many cases, more than one bundle from the stroma penetrated the epithelium at the same site, and no significant

differences were found in the distribution of epithelial nerve bundles in the four cornea quadrants (Fig. 3e). In Figure 3a, the nerve bundles converged into an area approximately 2 mm nasal and 1 mm inferior to the apex of the cornea. The convergence patterns and locations differed among samples. Among the seven eyes in which the converging patterns were studied, five eyes had merging points located in the inferior quadrant within the central zone, and two eyes had these points positioned in the inferior-nasal quadrant beyond the central zone. In addition, the convergence for four of the eyes was in a clockwise pattern, while three of the eyes had a counter-clockwise pattern. Figure 3e shows two representative images of the counter-clockwise patterns.

The montage of the corneal hemi-sections showed the transverse view of corneal epithelial innervations (Fig. 4). Highlighted images chosen from the center and periphery, which were counterstained with DAPI, revealed the detailed distribution of the network. The intraepithelial location of nerve bundles may be caused by the oblique sections. As mentioned, there was a large number of DCs stained with βIII-tubulin in the limbus.

3.3. Epithelial nerve densities and nerve terminals in human corneas

To investigate the distribution of epithelial nerves and nerve terminals, 10 human eyes from five donors; two females (ages 44 and 54 years old) and three males (ages 40, 45 and 57 years old) were chosen. Epithelial nerve density, calculated as the percentage of total area, was 18.78 ±2.06 in the central area and 11.05±2.27 in the peripheral area in the normal adult human corneas examined (Fig. 5a, b), with a significant difference of $p<0.001$. Nerve terminals, calculated as the number of terminals/mm^2 were also greater in the center (525±72) than in the periphery (230±46, $p< 0.001$, Fig. 5c, d).

3.4. Effect of gender and aging on corneal epithelial nerves

To examine the effect of gender on corneal epithelial nerves, we compared the epithelial nerve densities in the corneas of three male donors (ages 40, 45 and 57 years old) and two female donors (ages 44 and 54 years old). No differences in epithelial nerve densities were found between genders either in the central or in the peripheral epithelial nerves (Fig. 6a).

To examine the effect of aging on changes in epithelial nerve densities, we compared the central epithelial nerve densities in corneas of donors from the following age groups: 19 years old (two eyes); 40–54 years old (eight eyes); 63–67 years old (six eyes); and 75–80 years old (six eyes). A gradual decrease in central epithelial nerve density concomitant with increasing age was found, and a significant decrease ($p<0.01$) was observed in the corneas of 75- to 80-year-old donors compare to the 19-year old and the group of 40- to 54-year old donors (Fig. 6b, c). In the older corneas (>60 years), irregular lesions of nerve fibers were present in the superficial stroma beneath the basement membrane (Fig. 6e). These lesions were localized around the peripheral cornea in areas where the epithelial nerve bundles emerged. These anomalies were found more frequently in corneas of 75- to 80-year-old donors (17±3.6/cornea) as opposed to those of 60- to 67-year-old donors (7.8±3.0/ cornea).

4. Discussion

The methodological approach used in the present study allows us to show, for the first time, a complete view of the human corneal nerve distribution. Several factors contribute to our construction of this detailed map of the nerves. **First**, preparation of corneal whole mounts, without damaging the clear cornea by cutting or compressing the tissue, permitted visualization of the corneal nerves *in situ.* **Second**, marking the tissue before excising permitted acquisition of the precise position and distribution of nerves in each quadrant of the cornea. **Third**, using the same cornea for whole mount and cross-section examination – a novel technique developed

in our laboratory – allowed for precise location of nerve fibers within the cornea. Previous studies using cross-sections failed to show detailed corneal innervations. Nerve degeneration is thought to be the main reason behind this failure, because electron microscopy has shown signs of significant degeneration within 13.5 hours of death (Müller et al., 1996, 1997, 2003). However, this may not always be the case. All the corneas used in this study were kept in a wet chamber for an average of 36 hours before fixation, and they still retained their nerve structure, which allowed for quantification of the fine terminals, as shown in Figures 3d and 5d. This suggests that the conventional tissue processing used for immunochemistry may have had some effect on the nerves, resulting in nerve fibers being unstained or destroyed. **Fourth**, βIII-tubulin is a pan-neuronal marker that stains all the nerves in the cornea. The positive stains in the images represent the whole corneal nerve structures, regardless of their origins or phenotypes. Therefore, this marker is the optimal choice for studying the corneal nerve architecture in humans. **Finally**, the nerve density and nerve terminal data derived from the whole mount view of corneal nerves eliminates the variability associated with smaller samples and allows for the simultaneous evaluation of nerve density changes in different areas of the cornea.

Corneal stromal nerves were first described by Hoyer with the use of golden chloride staining, and subsequently identified by Dogiel with methylene blue and Cajal with silver chloride stains (Schimmelpfennig, 1982; Zander and Weddell, 1951). Since then, many studies have been performed, but a satisfactory description of the stromal nerve architecture in the human cornea remained unavailable. Our study confirms that human corneal stromal nerves enter in a radial pattern and run towards the anterior stroma (Zander and Weddell, 1951; Maurice; 1984), subsequently dividing into smaller branches to penetrate upwards into the epithelium and constitute the epithelial nerve network. In agreement with a more recent study (Marfurt et al., 2010), we also found that some of these branches connect with each other in the center of the stroma.

Quantitative analysis of corneal stromal nerve distribution has been performed in different species, including humans (Al-Aqaba et al. 2009; Ishida et al., 1984; Lasys et al. 2003; Marfurt et al., 2010; Zander and Weddell, 1951). Anywhere from 12 to 15 thick nerve bundles, which are equally distributed around the corneal limbus, have been reported in dogs (Lasys et al., 2003). A study by Zander and Weddell reported that there are about 70–90 nerve bundles entering the human cornea, but it is unclear whether they are epithelial nerve bundles or stromal nerves (Zander and Weddell, 1951). Two recent studies reported varying numbers of nerves in the human stroma: one reported 44 nerves, and the other 71 (Al-Aqaba et al. 2009; Marfurt et al., 2010). In the current study, we found an average of 33 stromal nerve bundles located at the corneo-scleral junction. The discrepancies between these studies may be due to differences in the points where the nerves were imaged and counted. As shown in the whole view image of the stromal nerves (Fig. 1d, g), the stromal nerves enter the cornea like a tree dividing into several branches in the peripheral area close to the limbus. Because the number of nerve divisions increases in relation to the distance from the corneo-scleral junction, more nerves will appear to be present than what are really in the cornea; as such, the starting point for nerve quantification should begin as close to the corneo-scleral junction as possible.

The existence of the epithelial nerve plexus has been known for more than a century since Cohnheim's original investigation (Schimmelpfennig, 1982), but the detailed architecture remained unclear and the exact location of this plexus was in dispute. Attias localized it above Bowman's membrane and reported that its fibers gradually ascended to the upper epithelium (Attias, 1912). Schimmelpfennig and Müller, however, reported that the plexus existed in the basal epithelial cell layer and introduced the terminology "subbasal plexus" (Schimmelpfennig, 1982; Müller et al., 1996). Our study shows that the plexus forms a delicate three-dimensional network in the corneal epithelium. We found two sources of nerve networks in the epithelium:

1) the limbal superficial nerve network (LSNN), which supplies the nerves for the limbal area and most of the peripheral area; and 2) the stromal nerve network, which supplies nerve branches to the central epithelia. In the central cornea, the long nerve bundles extend from the periphery to make up the skeleton of the network. Smaller divisions or nerve fibers branch out from the bundles and connect to each other, thus constructing the epithelial nerve network.

Earlier studies of corneal nerve densities have been performed primarily based on their sensitivity using Cochet-Bonnet esthesiometry (Darwish et al., 2007; Lawrenson and Ruskell, 1993; Roszkowska et al., 2004). Studies using IVCM reported an average of six to eight nerve bundles per image (about 0.1 mm^2 in size); based on this information, it has been estimated that there are approximately 5400–7200 nerve bundles in the human subbasal plexus (Rosenberg et al., 2000; Vesaluoma et al., 2000a, 2000b; Oliveira-Soto and Efron, 2001). By extrapolation, it has been predicted that there are between 300,000 and 630,000 free nerve endings in the cornea (Müller et al., 2003). In our study, taking into consideration the entire view of corneal epithelial innervation and by directly counting the bundles at the sites of epithelial perforation, we calculated an average of 351 nerve bundles per cornea. This number is between 15–20 times lower than that previously estimated in studies using IVCM.

We attribute this discrepancy to the imaging techniques employed. IVCM images of human corneas are recorded from the corneal apex, the area most densely innervated because of nerve bundle convergence, as shown in Figure 3. From the image of the whole cornea, we found that most of the bundles running from the periphery to the center divide into several branches that connect to each other in the central area. In addition, most IVCM studies depict the nerve fibers in either a 6–12 o'clock (superior-to-inferior) or in a 9-3 o'clock (temporal-to-nasal) orientation (Müller et al., 2003). If the images are acquired following only one direction, it is very likely that some of the bundles will be repeatedly recorded because of possible overlap that may occur at the edge of each image. Hence, the data derived from those images will produce a much higher number of nerve bundles than the ones reported in the current study.

In agreement with the distribution of stromal nerves, we also noted that there were no differences in the distribution of epithelial nerves in the four quadrants. These findings have clinical relevance because of the popularity of refractive surgery procedures that result in damage of the corneal nerves. Controversy has arisen in regards to the flap position in LASIK surgery procedures. Some ophthalmologists believe a horizontal flap is better than a vertical flap (Battat et al., 2001; Donnenfeld et al., 2003; Matsui et al., 2001; Perez-Santonja et al., 1999) while others think there is no difference (Ghoreishi et al., 2005; Mian et al., 2007; Vroman et al., 2005). The performance of a horizontal flap is supported by the model of corneal innervations proposing that the long ciliary nerves enter the cornea at the 3- and 9-o'clock positions (Müller et al., 1996, 1997), suggesting that there is greater susceptibility to corneal nerve damage with vertically- than horizontally-hinged flaps. Our findings that the distributions of both stromal nerves and the epithelial nerve bundles are not significantly different in each quadrant provide direct anatomical evidence to support that the position of the flap is irrelevant.

Nerve terminals, or free endings, are responsible for transducing sensory stimuli into nerve signals, and their numbers are directly proportional to corneal sensitivity (Belmonte et al., 2004). Earlier studies have shown that normal corneal sensitivity is higher in the center of the cornea than at the periphery (Millodot, 1977; Millodot and Larson, 1969; Roszkowska et al., 2004). Ultrastructural studies reported that the central cornea is five to six times more densely innervated than the peripheral cornea (Müller et al., 1997), but have not shown the distribution of the nerve terminals. When we compared the number of nerve terminals and the nerve fiber densities in the center and periphery of the cornea, we found a significantly higher density in the center. We concluded that the different sources of nerves supplied to the epithelium may

contribute to these differences in nerve densities. Although epithelial bundles emerged in the corneal periphery, most of the innervations were supplied by the superficial nerve network around the limbus. In comparison with the long bundles supplying the central cornea, these nerve fibers were shorter and smaller in size, and some areas had no visible nerve fibers.

There were no differences in epithelial nerve densities between corneas from males and females; this is in agreement with another recent study by Roszkowska *et al*. on corneal sensitivity (Roszkowska et al., 2004). Instead, we observed a progressive reduction in epithelial nerve densities with increasing aging, with a significant decline occurring in corneas of donors 70-years of age and older. Our results differ from the work of Marfurt et al., 2010, in which no correlation between sub basal nerve densities and donor age was found. In Marfurt's study, quantitative analysis was performed by schematic drawings of corneal nerves in the central cornea, while in our study we stained and measured the entire epithelial network. Studies with IVCM have shown either no change in human subjects aged 15 to 79 (Erie et al., 2005) or a decrease in epithelial nerve density between young and old corneas (Grupcheva et al., 2002; Benitez del Castillo et al., 2007).

The observed decrease was associated with nerve anomalies occurring in the peripheral cornea that damaged the epithelial nerve bundles at their points of emergence, thus leading to a reduction in the number of nerve bundle fibers. The exact mechanism in the formation of these nerve anomalies is unknown at present; however, the coincidence of these nerve lesions with arcus senilis in the pathological site and the age of onset imply that lipid deposition may have a role in its pathogenesis (Sheraidah et al., 1981; Crispin, 2002). Clinical studies reported that incidence of dry eye increase significantly with age (Smith, 2007). The age-related decrease in corneal innervation disrupts the reflex circuits that drive blinking and lacrimation and also diminishes essential corneal nerve-supplied throphic factors, thus leading to diminished corneal sensitivity, dry eye and impaired wound healing.

One interesting finding was the positive staining of dendritic cells with βIII tubulin (Tuj1, a monoclonal antibody specific for neuronal class βIII tubulin). These cells have been known to be present in the human cornea ever since Langerhans first observed them in human skin stained with golden chloride (Langerhans et al., 1868; Merad, 2008). Schimmelpfennig showed the existence of these cells in the central epithelium of diseased corneas (Schimmelpfennig, 1982). Recent studies with IVCM have reported the presence of DCs in the central and inferior periphery of normal and pathological human corneas (Kawamoto et al., 2009; Patel and McGhee, 2005; Zhivov et al., 2005). In our study of normal corneas, DCs were predominantly present in the peripheral epithelium around the limbal area and in the conjunctival epithelium, but were rarely seen in the clear cornea. Dendritic cells are known for their immunological functions and have been implicated in corneal inflammation and dry eye (Hamrah et al., 2002; Tuisku et al., 2008). Although they were positively stained with βIII-tubulin in the current study, dendritic cells seemed to have little contact with the corneal nerves. Further experiments will need to be conducted to clarify their roles.

In conclusion, using a modified method of immunofluorescence staining and imaging, we constructed, for the first time, a three-dimensional map of the entire architecture of the human corneal nerves in both the epithelium and the stroma. We calculated the epithelial nerve density and the number of nerve terminals in different parts of the cornea and determined the effects of aging and gender on changes in central corneal epithelial nerve densities. The findings in this study not only provide comprehensive information of human corneal innervation, but also have clinical implications in wound healing, dry eye, and other ocular disorders related to neurothrophic keratitis.

Acknowledgments

Supported by R01EY019465 from the National Eye Institute. The content is solely the responsibility of the authors and does not necessarily represent the official view of the National Eye Institute or the National Institutes of Health.

References

Al-Aqaba M, Fares U, Suleman H, Lowe J, Dua HS. Architecture and distribution of human corneal nerves. Br J Ophthalmol. 2009 In press.

Attias G. Die Nerven der Hornhaut des Menschen. Albrecht von Graefes Arch Klin Exp Ophthalmol 1912;83:207–316.

Auran JD, Koester CJ, Kleiman NJ, Rapaport R, Bomann JS, Wirotsko BM, Florakis GJ, Koniarek JP. Scanning slit confocal microscopic observation of cell morphology and movement within the normal human anterior cornea. Ophthalmology 1995;102:33–41. [PubMed: 7831039]

Battat L, Macri A, Dursun D, Pflugfelder SC. Effects of laser in situ keratomileusis on tear production, clearance, and the ocular surface. Ophthalmology 2001;108:1230–1235. [PubMed: 11425680]

Belmonte C, Acosta MC, Gallar J. Neural basis of sensation in intact and injured corneas. Exp Eye Res 2004;78:513–525. [PubMed: 15106930]

Benítez-Del-Castillo JM, Acosta MC, Wassfi MA, Díaz-Valle D, Gegúndez JA, Fernandez C, García-Sánchez J. Relation between corneal innervation with confocal microscopy and corneal sensitivity with noncontact esthesiometry in patients with dry eye. Invest Ophthalmol Vis Sci 2007;48:173–181. [PubMed: 17197530]

Cortina MS, He J, Li N, Bazan NG, Bazan HE. Neuroprotectin D1 synthesis and corneal nerve regeneration after experimental surgery and treatment with PEDF plus DHA. Invest Ophthalmol Vis Sci 2010;51:804–810. [PubMed: 19797230]

Crispin S. Ocular lipid deposition and hyperlipoproteinaemia. Prog Retin Eye Res 2002;21:169–224. [PubMed: 12062534]

Darwish T, Brahma A, O'Donnell C, Efron N. Subbasal nerve fiber regeneration after LASIK and LASEK assessed by noncontact esthesiometry and in vivo confocal microscopy: prospective study. J Cataract Refract Surg 2007;33:1515–1521. [PubMed: 17720064]

Donnenfeld ED, Solomon K, Perry HD, Doshi SJ, Ehrenhaus M, Solomon R, Biser S. The effect of hinge position on corneal sensation and dry eye after LASIK. Ophthalmology 2003;110:1023–1029. [PubMed: 12750107]

Erie JC, McLaren JW, Hodge DO, Bourne WM. The effect of age on the corneal subbasal nerve plexus. Cornea 2005;24:705–709. [PubMed: 16015090]

Esquenazi S, Bazan HE, Bui V, He J, Kim DB, Bazan NG. Topical combination of NGF and DHA increases rabbit corneal nerve regeneration after photorefractive keratectomy. Invest Ophthalmol Vis Sci 2005;46:3121–3127. [PubMed: 16123410]

Ghoreishi M, Aidenloo NS, Peyman A, Peyman M, Haghdoustoskoey M. Does hinge position affect dry eye after laser in situ keratomileusis? Ophthalmologica 2005;219:276–280. [PubMed: 16123553]

Grupcheva CN, Wong T, Riley AF, McGhee CN. Assessing the sub-basal nerve plexus of the living healthy human cornea by in vivo confocal microscopy. Clin Experiment Ophthalmol 2002;30:187–190. [PubMed: 12010212]

Hamrah P, Zhang Q, Liu Y, Dana MR. Novel characterization of MHC class II- negative population of resident corneal Langerhans cell-type dendritic cells. Invest Ophthalmol Vis Sci 2002;43:639–646. [PubMed: 11867578]

He J, Bazan NG, Bazan HEP. Mapping the whole human corneal nerve architecture. ARVO. 2009 May 3–7; E-abstract: 2603-D1023.

Ishida N, del Cerro M, Rao GN, Mathe M, Aquavella JV. Corneal stromal innervation. A quantitative analysis of distribution. Ophthalmic Res 1984;16:139–144. [PubMed: 6472793]

Kawamoto K, Chikama T, Takahashi N, Nishida T. In vivo observation of Langerhans cells by laser confocal microscopy in Thygeson's superficial punctate keratitis. Mol Vis 2009;15:1456–1462. [PubMed: 19649162]

Langerhans P. Ueber die Nervender menschlicher. Haut Virchows Arch 1868;44:325.

Lasys V, Stanevicius E, Zamokas G. Evaluation of peculiarities of the acetylcholinesterase-positive nerve plexus and its length in the cornea. Medicina 2003;39:955–959. [PubMed: 14578637]

Lawrenson JG, Ruskell GL. Investigation of limbal touch sensitivity using a Cochet-Bonnet aesthesiometer. Br J Ophthalmol 1993;77:339–343. [PubMed: 8318479]

Lee BH, McLaren JW, Erie JC, Hodge DO, Bourne WM. Reinnervation in the cornea after LASIK. Invest Ophthalmol Vis Sci 2002;43:3660–3664. [PubMed: 12454033]

Malik RA, Kallinikos P, Abbott CA, van Schie CH, Morgan P, Efron N, Boulton AJ. Corneal confocal microscopy: a non-invasive surrogate of nerve fibre damage and repair in diabetic patients. Diabetologia 2003;46:683–688. [PubMed: 12739016]

Marfurt CF, Cox J, Deek S, Dvorscak L. Anatomy of the human corneal innervation. Exp Eye Res 2010;90:478–492. [PubMed: 20036654]

Matsui H, Kumano Y, Zushi I, Yamada T, Matsui T, Nishida T. Corneal sensation after correction of myopia by photorefractive keratectomy and laser in situ keratomileusis. J Cataract Refract Surg 2001;27:370–373. [PubMed: 11255047]

Maurice, DM. The Cornea and Sclera. In: Davson, H., editor. In The Eye. Academic Press; New York: 1984. p. 1-158.

Merad M, Ginhoux F, Collin M. Origin, homeostasis and function of Langerhans cells and other langerin-expressing dendritic cells. Nat Rev Immunol 2008;8:935–947. [PubMed: 19029989]

Mian SI, Shtein RM, Nelson A, Musch DC. Effect of hinge position on corneal sensation and dry eye after laser in situ keratomileusis using a femtosecond laser. J Cataract Refract Surg 2007;33:1190–1194. [PubMed: 17586374]

Millodot M. The influence of age on the sensitivity of the cornea. Invest Ophthalmol Vis Sci 1977;16:240–242. [PubMed: 844979]

Millodot M, Larson W. New measurements of corneal sensitivity: a preliminary report. Am J Optom Arch Am Acad Optom 1969;46:261–265. [PubMed: 5253423]

Müller LJ, Pels L, Vrensen GF. Ultrastructural organization of human corneal nerves. Invest Ophthalmol Vis Sci 1996;37:476–488. [PubMed: 8595948]

Müller LJ, Vrensen GF, Pels L, Cardozo BN, Willekens B. Architecture of human corneal nerves. Invest Ophthalmol Vis Sci 1997;38:985–994. [PubMed: 9112994]

Müller LJ, Marfurt CF, Kruse F, Tervo TM. Corneal nerves: structure, content and function. Exp Eye Res 2003;76:521–542. [PubMed: 12697417]

Oliveira-Soto L, Efron N. Morphology of corneal nerves using confocal microscopy. Cornea 2001;20:374–384. [PubMed: 11333324]

Patel DV, McGhee CN. Mapping of the normal human corneal sub-Basal nerve plexus by in vivo laser scanning confocal microscopy. Invest Ophthalmol Vis Sci 2005;46:4485–4488. [PubMed: 16303938]

Patel DV, McGhee CN. In vivo confocal microscopy of human corneal nerves in health, in ocular and systemic disease, and following corneal surgery: a review. Br J Ophthalmol 2009;93:853–860. [PubMed: 19019923]

Pérez-Santonja JJ, Sakla HF, Cardona C, Chipont E, Alió JL. Corneal sensitivity after photorefractive keratectomy and laser in situ keratomileusis for low myopia. Am J Ophthalmol 1999;127:497–504. [PubMed: 10334340]

Rosenberg ME, Tervo TM, Immonen IJ, Müller LJ, Grönhagen-Riska C, Vesaluoma MH. Corneal structure and sensitivity in type 1 diabetes mellitus. Invest Ophthalmol Vis Sci 2000;41:2915–2921. [PubMed: 10967045]

Roszkowska AM, Colosi P, Ferreri FM, Galasso S. Age-related modifications of corneal sensitivity. Ophthalmologica 2004;218:350–355. [PubMed: 15334017]

Scarpa F, Grisan E, Ruggeri A. Automatic recognition of corneal nerve structures in images from confocal microscopy. Invest Ophthalmol Vis Sci 2008;49:4801–4807. [PubMed: 18614801]

Schimmelpfennig B. Nerve structures in human central corneal epithelium. Graefes Arch Clin Exp Ophthalmol 1982;218:14–20. [PubMed: 7056476]

Schlemm TFW. Nerven der Cornea. Ammon' Z Ophthalmol 1831;1:113–114.

Sheraidah GA, Winder AF, Fielder AR. Lipid-protein constituents of human corneal arcus. Atherosclerosis 1981;40:91–98. [PubMed: 7284055]

Smith JA. The epidemiology of dry eye disease: report of the epidemiology subcommittee of the international dry eye workshop (2007). Ocul Surf 2007;5:93–107. [PubMed: 17508117]

Stachs O, Zhivov A, Kraak R, Stave J, Guthoff R. In vivo three-dimensional confocal laser scanning microscopy of the epithelial nerve structure in the human cornea. Graefes Arch Clin Exp Ophthalmol 2007;245:569–575. [PubMed: 16941142]

Tuisku IS, Konttinen YT, Konttinen LM, Tervo TM. Alterations in corneal sensitivity and nerve morphology in patients with primary Sjögren's syndrome. Exp Eye Res 2008;86:879–885. [PubMed: 18436208]

Ueda S, del Cerro M, LoCascio JA, Aquavella JV. Peptidergic and catecholaminergic fibers in the human corneal epithelium. An immunohistochemical and electron microscopic study. Acta Ophthalmol Suppl 1989;192:80–90. [PubMed: 2573227]

Vera LS, Gueudry J, Delcampe A, Roujeau JC, Brasseur G, Muraine M. In vivo confocal microscopic evaluation of corneal changes in chronic Stevens-Johnson syndrome and toxic epidermal necrolysis. Cornea 2009;28:401–407. [PubMed: 19411958]

Vesaluoma M, Pérez-Santonja J, Petroll WM, Linna T, Alió J, Tervo T. Corneal stromal changes induced by myopic LASIK. Invest Ophthalmol Vis Sci 2000a;41:369–376. [PubMed: 10670464]

Vesaluoma M, Müller L, Gallar J, Lambiase A, Moilanen J, Hack T, Belmonte C, Tervo T. Effects of oleoresin capsicum pepper spray on human corneal morphology and sensitivity. Invest Ophthalmol Vis Sci 2000b;41:2138–2147. [PubMed: 10892855]

Vroman DT, Sandoval HP, Fernández de Castro LE, Kasper TJ, Holzer MP, Solomon KD. Effect of hinge location on corneal sensation and dry eye after laser in situ keratomileusis for myopia. J Cataract Refract Surg 2005;31:1881–1887. [PubMed: 16338555]

Zander E, Weddell G. Observations on the innervation of the cornea. J Anat 1951;85:68–99. [PubMed: 14814019]

Zhivov A, Stave J, Vollmar B, Guthoff R. In vivo confocal microscopic evaluation of Langerhans cell density and distribution in the normal human corneal epithelium. Graefes ArchClin Exp Ophthalmol 2005;243:1056–1061.

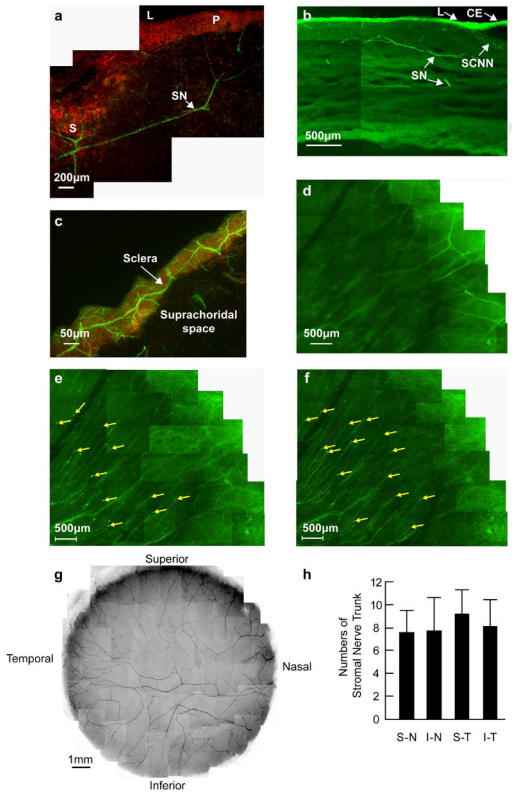

Figure 1. The origin and location of corneal stromal nerves

(**a**) Transverse section showing the course of nerve fibers running from the sclera to the peripheral corneal stroma. DAPI (red) was used to stain the nuclei. S: sclera; L: limbus; P: periphery; SN: stromal nerves. (**b**) Location of stromal nerves in the limbal area and peripheral cornea. CE: conjunctival epithelium; SCNN: Sub-conjunctival nerve network; L: limbus; SN: Stromal nerves. (**c**) Horizontal section showing scleral nerves along the limbus at the sclera side. (**d-f**) Whole mount view of corneal nerves in the limbal and peripheral cornea in the superior-temporal quadrant. (**d**) Deep stromal nerves, which divide into several branches upon entering the cornea. (**e**) Transition of stromal nerves to epithelial nerves. (**f**) Epithelial nerves. The tips are perforation points of the stromal nerves in the epithelium. (**g**) Whole mount view of human corneal stromal nerve network. The images were taken with a Nikon SMZ-1500 stereo microscope and a 4× lens from the right eye of a 45-year-old male donor. (**h**) Distribution of stromal nerve main branches in the four quadrants of the human corneas. The position of each quadrant was marked before removal of the cornea, as explained in Materials and methods. The number of stromal nerves from 10 corneas (ages 40–57 years old) were counted at the corneo-scleral junction with a Nikon SMZ-1500 stereo microscope. Data expressed as average ± SD.

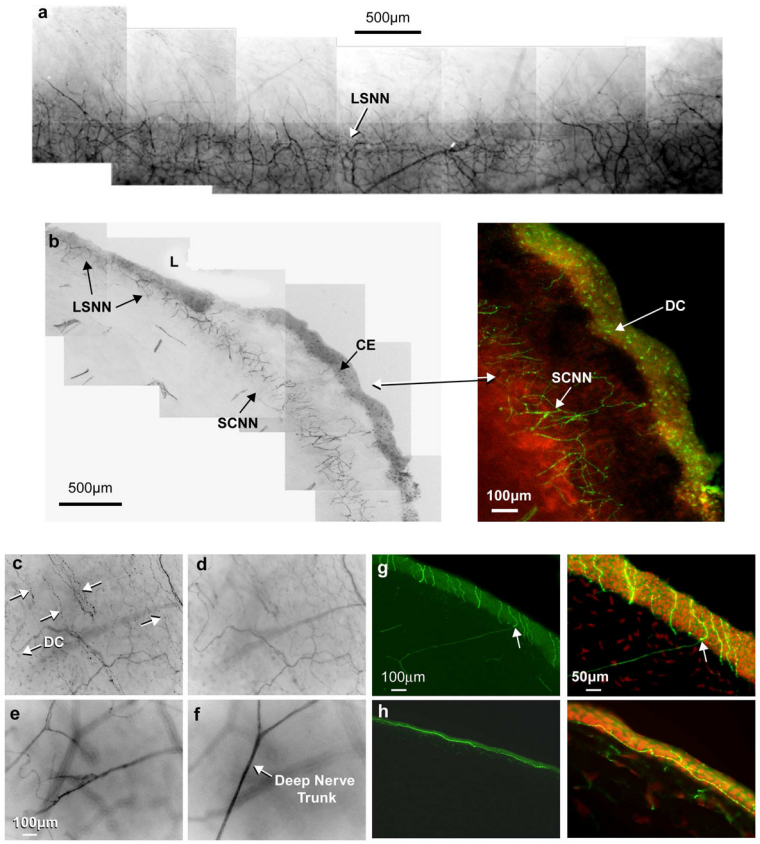

Figure 2. Origin of corneal epithelial nerves

(**a**) Whole mount view of the limbal superficial nerve network (LSNN), which surrounds the corneal limbus and extends from the sub-conjunctival nerve network (SCNN). (**b**) Transected view of the LSNN and SCNN. Inset shows numerous dendritic cells (DC) present in the conjunctival epithelium (CE). (**c-f**) Montages of stacks showing the nerves at the limbal area at different depths. Arrows indicate the fine nerve bundles at the superficial layer and numerous DCs. (**g**) Epithelial nerves derived from the stromal branches. The transected view shows the perforating sites of stromal nerve branch tips (arrows). (**h**) Perpendicular section from the cornea of the 19–year-old donor shows the epithelial nerve bundles running horizontal in the epithelium close to the basal cells. DAPI was used to stain the nuclei.

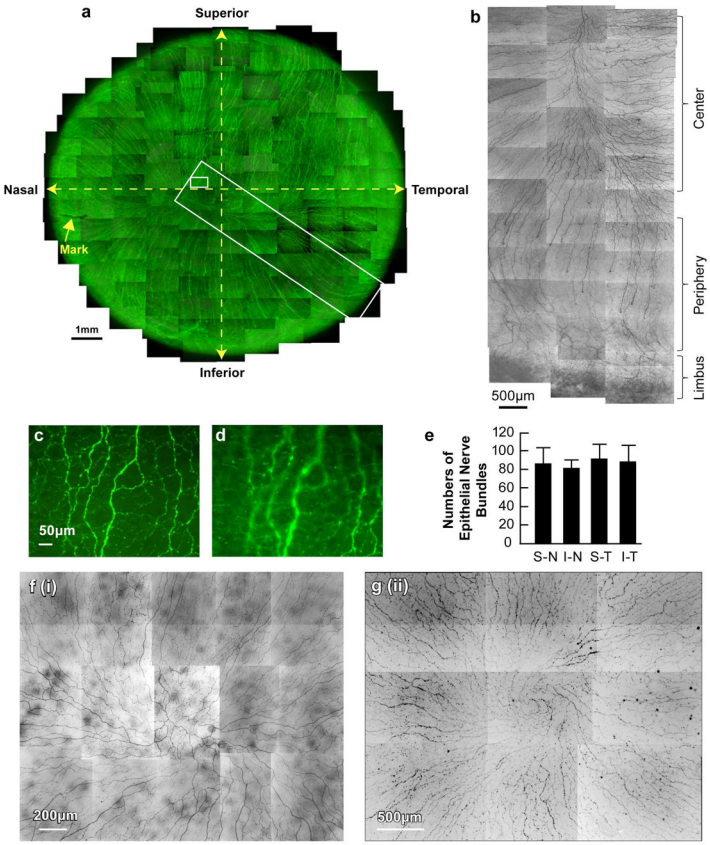

Figure 3. Whole mount view of corneal epithelial nerve network

(**a**) Images were acquired in a time-lapse mode with a Nikon Eclipse TE200 and with a 10× lens in compliance with the natural shape of cornea obtained from the left eye of a 45-year-old male donor. More than a thousand stacks were merged together to construct the whole view of the distribution of corneal epithelial nerves. (**b-d**) Details of two chosen areas of the cornea. **(b)** Detailed course of epithelial nerve bundles running from the periphery to convergence at the center of the cornea. (**c**) Detailed structure of the epithelial nerve network in the center. (**d**) Image from the same frame as **b**, but with a different focus to show the epithelial nerve terminals. (**e**) Distribution of epithelial nerve bundles in the four quadrants. The numbers of epithelial nerve bundles were counted from seven human corneas (ages 40, 44, 45 and 54 years old) based on the whole mount view. Data expressed as average ±SD. **(f)**. Representative patterns of convergence taken from a 54-year-old female (i) and a 63-year-old male (ii).

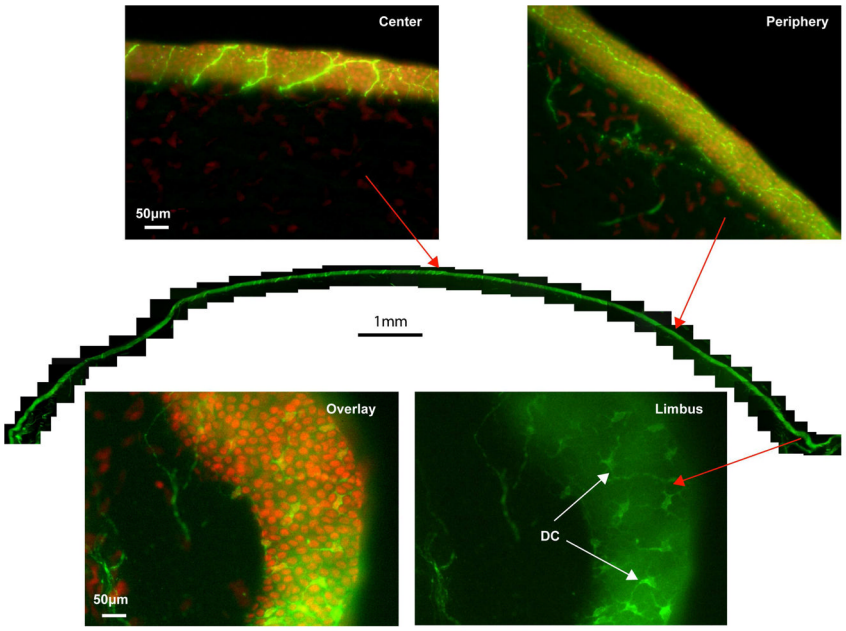

Figure 4. Transected view of the entire epithelial nerve network

For the reconstruction, the same cornea as in Figure 3 was used. Representative images from the whole view montage, counterstained with DAPI, show the features of epithelial nerves at the center and periphery. In the limbal area, numerous dendritic cells stained with βIII-tubulin are visible.

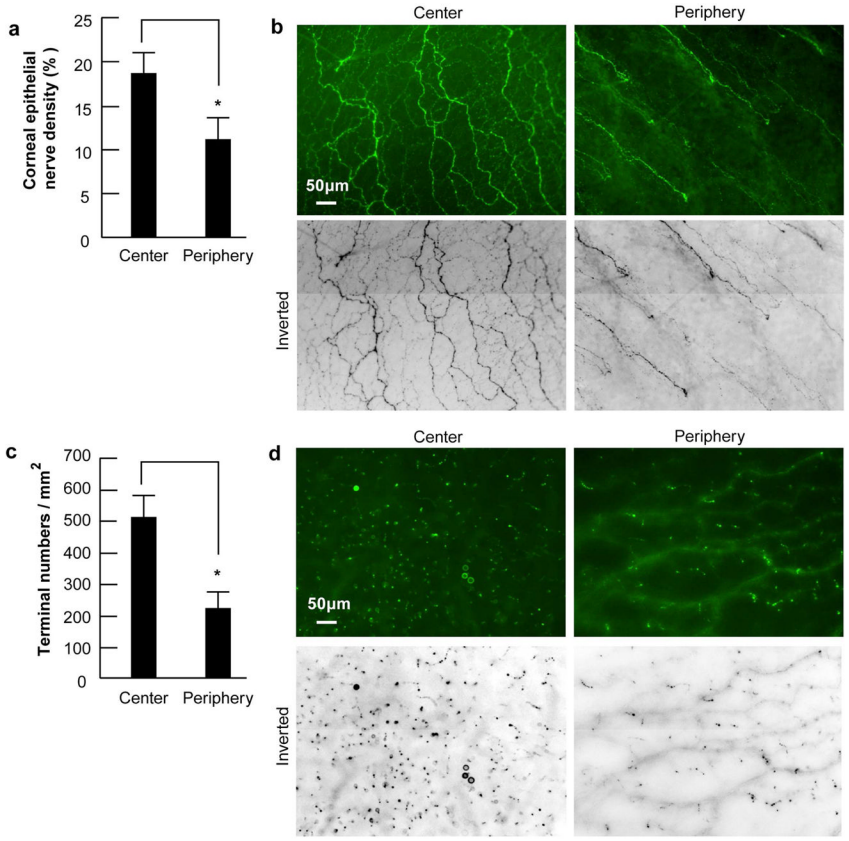

Figure 5. Difference of corneal epithelial nerve density and nerve terminals between the central and the peripheral zone

(**a**) Nerve density in human corneas was calculated as percentage of total area in each image. Eighty images for each zone from 10 corneas were used. Data expressed as average ± SD. * $p < 0.001$ (**b**) Representative images of central and peripheral epithelial nerves. (**c**) Number of nerve terminals. Forty images for each zone from 10 corneas were used. The terminal numbers in each image were directly counted. Because each image took up an area of 0.335 mm^2, the terminal numbers per mm^2 were calculated. Data expressed as average ± SD. $p<0.001$. (**d**) Representative images of nerve terminals taken from a 52–year-old male donor from the center and the periphery zones.

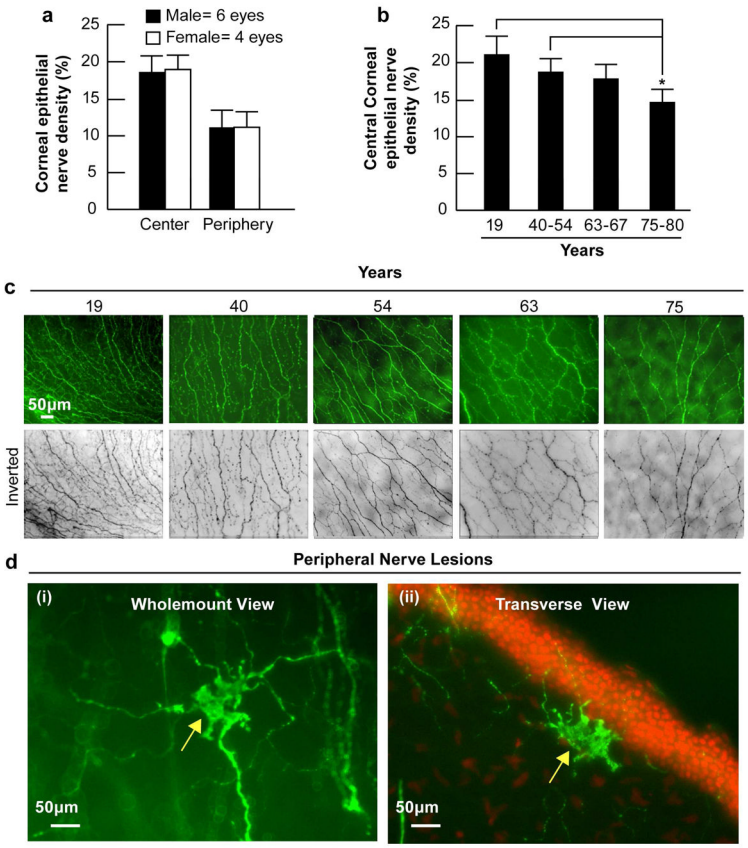

Figure 6. Effect of gender and aging in corneal epithelial nerve density

(**a**) Sixty-four images (32 images for each zone) from four female corneas and 96 images (48 images for each zone) from six male corneas were used. (**b**) Eight images were recorded from the central zone of each cornea. Forty-eight images from each group were used for analysis, except for the 19-year-old group in which there were only 16 images from the central zone. Data expressed as average ± SD. Differences of central corneal nerve densities between the groups were compared by analysis of variance (ANOVA). *$p < 0.05$. (**c**) Representative whole mount images of the central cornea from different age donors. (**d**) Morphology and location of peripheral neuropathies in a cornea of a 75-year-old donor. i) Whole mount view of neuropathy. ii) Transected view showing the nerve lesion localized in the anterior stroma beneath the epithelial basement membrane.